

# Thermal and ventilation modelling of large highly-glazed spaces

Anne Voeltzel\*, François Rémi Carrié, Gérard Guarracino

*Ecole Nationale des Travaux Publics de l'Etat, Laboratoire des Sciences de l'Habitat, Département Génie Civil et Bâtiment-URA CNRS 1652, Rue Maurice Audin, 69518 Vaulx-en-Velin Cedex, France*

Received 21 January 2000; accepted 7 July 2000

## Abstract

Highly-glazed spaces are attractive in many ways (solar heating, aesthetics, etc.), however, their thermal behaviour remains difficult to predict. In such spaces, the assumptions or methods generally used in building thermal simulation tools — e.g. homogeneous air temperature in the room, simplified calculations of radiative heat transfer between walls, absence of airflow modelling within the room — do not seem appropriate. We have developed a new model (AIRGLAZE) to improve the prediction of the thermal behaviour of large highly-glazed spaces. It consists of an envelope module to calculate conductive and radiative heat transfer in the building envelope. It is coupled with a zonal airflow model to predict air motion within the room. Particular attention is paid to sun patch modelling and the internal distribution of shortwave and longwave radiation within the building; direct retransmission, reflection to the outside, and transmission to other zones of the building are taken into account. The results of AIRGLAZE are compared with measurement data from two experimental test cells: the IEA Annex 26 experimental atrium, and a test cell at ENTPE. Compared to the one-air-node approach, the zonal method significantly reduces the mean discrepancy with measurement data during stratified conditions (from 3.9°C down to 0.4°C for the Annex 26 atrium). In general, experimental and numerical results tally well in both cases. © 2001 Elsevier Science B.V. All rights reserved.

**Keywords:** Large highly-glazed spaces; AIRGLAZE; Ventilation modelling; Zonal model; Commercial buildings; Energy; Heat transfer

## 1. Introduction

Highly-glazed buildings are attractive in many ways. They virtually open the building to the outside while protecting the occupants from the outdoor climate. This sociological feature is very important to architects who are usually concerned about the symbolic meaning of different design alternatives. Also, they provide daylight to the occupants, which can be both pleasant and save energy [1,2].

The glass industry has made tremendous progress within the past two decades with respect to the thermal and optical properties of glazings. Nowadays, windows with  $U$ -values lower than  $2.0 \text{ W m}^{-2} \text{ C}^{-1}$  and variable transmission glazings are commercially available. Along with improvements with respect to structural design and installation, technological progress in this field makes the use of glass more and more popular on a large scale. However, most highly-glazed spaces appear to have major design flaws that lead to considerable energy wastage and discomfort. It is estimated

that the energy consumption (normalised by floor-area) of such service buildings lies in the region of 250–300  $\text{kW h m}^{-2}$  per year for European countries whereas, with good design, it is reasonable nowadays to aim for energy consumption lower than 150  $\text{kW h m}^{-2}$  per year. Furthermore, energy-expensive remedies, e.g. using active cooling strategies — are considered by designers more and more, although they can rarely overcome the violation of simple design rules regarding, for example, ventilation or solar protections. Thus, energy use and comfort issues are often either inadequately addressed or discarded, especially at the early stages of design.

One major reason for these design problems certainly lies in the lack of adequate design tools for such spaces. Pfrommer [3] simulated a building with a south-facing glazed conservatory and focused on the size of the window separating the conservatory from the rest of the building. He based his analyses on two commonly-used dynamic thermal simulation tools — Esp-r [4] and HTB2 [5] with different modelling options regarding the internal distribution of solar radiation and the thermal model of glazings (total of six simulations). His sensitivity analysis on the size of the separating window showed increasing or decreasing energy consumption depending on which modelling option and/or

\* Corresponding author. Tel.: +33-4-72-14-33-99; fax: +33-4-72-14-34-70  
E-mail addresses: anne.voeltzel@equipement.gouv.fr (A. Voeltzel),  
remi.carrie@entpe.fr (F.R. Carrié), gerard.guarracino@entpe.fr  
(G. Guarracino).

**Nomenclature**

$A$	Area of interface ( $\text{m}^2$ )
$C_{ij}$	Empirical coefficient characterising the interface separating the control volume $i$ from the control volume $j$ ( $\text{m s}^{-1} \text{Pa}^{-n}$ )
$C_p$	Specific heat capacity of air ( $\text{J kg}^{-1} \text{C}^{-1}$ )
$F_{ki}$	View factor from surface $k$ to surface $i$
$g$	Gravitational acceleration ( $\text{m s}^{-2}$ )
$G_{ij}$	Gebhart's exchange factor from face $i$ to face $j$
$h$	Height of control volume (m)
$h_c$	Convective heat transfer coefficient at the wall ( $\text{W m}^{-2} \text{C}^{-1}$ )
$N$	Total number of interior surfaces in the room
$P$	Pressure in the control volume (Pa)
$Q$	Diffuse shortwave net flux incident on surface (W)
$Q_e$	Total shortwave diffuse flux source term of surface (W)
$Q_f$	Diffuse flux coming from the outside and transmitted to inside through the surface (W)
$Q_{ij}$	Mass airflow going from control volume $j$ to control volume $i$ . $Q_{ij} > 0$ if the flow is going from $j$ to $i$ ( $\text{kg s}^{-1}$ )
$Q_{\text{ref}}$	Reflected part of the direct incident shortwave flux (W)
$Q_s$	Airflow source in the control volume. $Q_s > 0$ if it is a source, and $Q_s < 0$ if it is a sink ( $\text{kg s}^{-1}$ )
$T$	Air temperature in control volume ( $^{\circ}\text{C}$ )
$T_{s,i}$	Air temperature of source or sink airflow in control volume $i$ . In case of a sink, $T_{s,i}$ is equal to the air temperature in the cell $i$ . In case of a source, $T_{s,i}$ is equal to the temperature of the air supplied in the control volume $i$ ( $^{\circ}\text{C}$ )
$T_{\text{wall}}$	Surface temperature of the interior face of the wall ( $^{\circ}\text{C}$ )
$V$	Volume of control volume ( $\text{m}^3$ )

**Greek symbols**

$\alpha$	Absorption coefficient for radiation
$\delta_{ij}$	Kronecker symbol: if $i = j$ , $\delta_{ij} = 1$ and if $i \neq j$ , $\delta_{ij} = 0$
$\varepsilon$	Longwave radiation emissivity
$\varepsilon_{ij}$	Sign of $P_j - P_i$ , $\varepsilon_{ij} = 1$ if ( $P_j > P_i$ ) and $\varepsilon_{ij} = -1$ if ( $P_j < P_i$ )
$\Phi_{\text{cond}}$	Conductive heat flux received by the control volume from neighbouring control volumes (W)
$\Phi_{\text{LW}}$	Net longwave flux absorbed by surface (W)
$\Phi_{\text{source}}$	Heat source (W)
$\rho$	Air density ( $\text{kg m}^{-3}$ )
$\rho$	Reflection coefficient for radiation
$\sigma_o$	Stefan–Boltzmann constant ( $=5.68 \times 10^{-8}$ ) ( $\text{W m}^{-2} \text{K}^{-4}$ )

**Subscripts**

d	Relative to direct solar radiation
f	Relative to diffuse solar radiation
$i$	Relative to control volume or wall face $i$
$ij$	Relative to interface separating control volume $i$ from control volume $j$
LW	Relative to longwave radiation
SW	Relative to shortwave radiation

program was used. These erroneous results can be explained by the poor modelling of some physical phenomena that is usually sufficient in conventional buildings. (Note that these building simulation codes were originally developed to study buildings with ordinary window sizes and volume.) This is, namely, that there are a number of simplifying assumptions regarding shortwave (SW) and longwave (LW) radiation heat transfer that cannot be applied to highly-glazed spaces. A significant fraction of the solar radiation entering a large highly-glazed room can be lost by direct transmission to the outside, direct transmission to other zones of the building, or diffuse retransmission to the outside (Fig. 1). Based on accurate radiative heat transfer simulations of four highly-glazed spaces, Wall [6] proved that 10–70% of the incoming solar radiation could be lost by retransmission. According to Wall [6], this fraction typically falls to 0–5% for conventional buildings. Serres [7] and Trombe et al. [8] report retransmission fractions of about 18% for a standard office room with one south-east facing window and one south-west.

Standard thermal building simulation codes generally assume that a room can be treated as a single zone with homogeneous air temperature. Clearly, this does not apply to large highly-glazed spaces. First, buoyancy-driven flows are known to be significant in such buildings, even when mechanical ventilation is used. Large volumes often lead to heterogeneous air temperature and velocity fields within the room. Besides, using an average air temperature on the

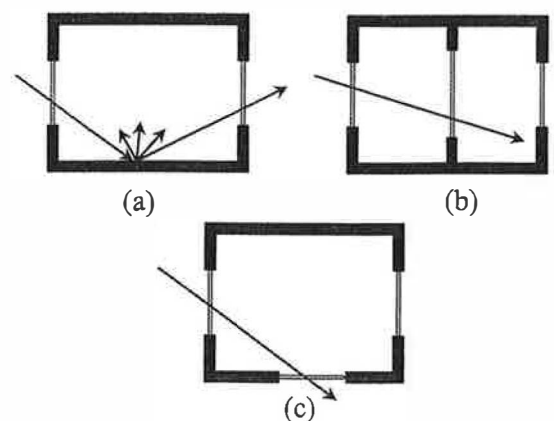


Fig. 1. (a) Reflection to the outside; (b) Transmission to other zones; (c) Direct retransmission.

total volume as a yardstick poses problems as the occupied zone represents only a small part of the total volume.

Laouadi and Atif [9] tried to better model highly-glazed spaces with Esp-r by splitting the air volume in thermal zones separated by fictitious walls. We made similar attempts with TRNSYS Type 56 [10]. Unfortunately, the choice of thermal and radiative characteristics of the fictitious walls has fundamental shortcomings. Namely, the radiative model of Esp-r does not take longwave radiative heat exchanges between surfaces belonging to different thermal zones into account [11]. In the TRNSYS Type 56, interior walls are internally set as opaque to shortwave and longwave radiation.

Many researchers and designers have used Navier–Stokes based computational fluid dynamic (CFD) to compute airflows inside buildings. Nevertheless, it remains a challenge to adequately use a CFD code to predict thermal and ventilation behaviour in a room, in particular in large volumes such as atria [12]. Tentative explanations are listed hereafter. First, the capabilities of CFD to describe buoyancy-driven flows in large enclosures have not yet been validated. Second, the very detailed input data necessary to the CFD is not consistent with the data usually available at the design stage of a building. Third, CFD simulations of large highly-glazed spaces remain mostly restricted to steady-state simulations because of the already huge computational effort needed [13,14].

Large highly-glazed spaces are subjected to rapid changes in insolation as the sun is viewed at different angles over the course of a day, and may be hidden by fixed or moving obstructions, e.g. buildings or clouds. Therefore, transient approaches appear essential to evaluate the thermal performances of such buildings. However, studies of large highly-glazed spaces in transient conditions including (a) a detailed calculation of shortwave and longwave radiative heat transfer, and (b) an airflow simulation, have never been reported in the literature.

The objectives of this research are (a) to develop a model for predicting the thermal and ventilation behaviour of large highly-glazed spaces in transient conditions, (b) to compare the simulation results with field data, and (c) to evaluate the added-value of modelling airflows within the space through a zonal approach. Field monitoring results that are used include those of (a) the atrium building studied within IEA Annex 26 [15], and (b) an experimental test cell at ENTPE instrumented for that purpose.

## 2. Modelling approaches

Our methodology consisted of developing (a) a zonal module to calculate the air temperature and velocity field within the room, and (b) an envelope module to calculate the surface temperatures that includes a sun patch model as well as adequate LW and SW radiation heat transfer models. Our simulation code (AIRGLAZE) is based on the coupling of

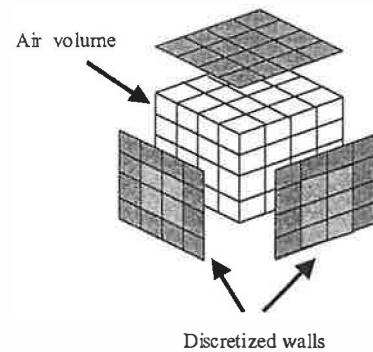


Fig. 2. Discretization of the air volume and walls.

these two modules. The air volume is cut into control volumes, and each wall of the envelope is discretized into several surfaces; this way, one interior surface of the envelope model is connected with one air temperature node of the airflow module (Fig. 2). The program was developed and implemented in the object-oriented C++ language and runs on a PC [11].

### 2.1. Airflow model

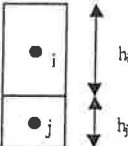
The zonal airflow model is based on a discretization of the air volume in control volumes in which pressure, air density, and air temperature are supposed to be uniform. These control volumes are connected by airflows induced by pressure differences between control volumes. The zonal model solves the mass balance equation (Eq. (1)), the enthalpy balance equation (Eq. (2)), and the perfect gas law equation of each control volume of the computational domain. This enables us to extract the unknown airflows between control volumes, as well as air temperature and density in each control volume. Note that no momentum equation is given, which means that momentum-driven zones, e.g. jet zones are usually poorly modelled.

$$\sum_j Q_{ij} + Q_{s,i} = 0 \quad (1)$$

$$\sum_{j, Q_{ij}>0} Q_{ij} C_p T_j + \sum_{j, Q_{ij}<0} Q_{ij} C_p T_i + \sum_{\text{walls}} h_{c,i} A_{i,\text{wall}} (T_{\text{wall}} - T_i) + Q_{s,i} C_p T_{s,i} + \Phi_{\text{source},i} + \Phi_{\text{cond},i} - \rho_i V_i C_p \frac{\partial T_i}{\partial t} = 0 \quad (2)$$

The mass airflow rates are derived from the pressures at the centres of the adjacent control volumes with a power law commonly used to describe the flow through small openings (Eq. (3); [16]). The flow through the interface of two adjacent control volumes is assumed to be monodirectional. For horizontal interfaces, the change in potential energy between the control volumes is taken into account, which leads to Eq. (4):

$$Q_{ij} = \varepsilon_{ij} C_{ij} A_{ij} \left\{ \frac{(1 - \varepsilon_{ij})}{2} \rho_i + \frac{(1 + \varepsilon_{ij})}{2} \rho_j \right\} |P_i - P_j|^n \quad (3)$$

$$Q_{ij} = \varepsilon_{ij} C_{ij} A_{ij} \left\{ \frac{(1 - \varepsilon_{ij})}{2} \rho_i + \frac{(1 - \varepsilon_{ij})}{2} \rho_j \right\} \times \left| P_i - P_j + \frac{1}{2} (\rho_i g h_i + \rho_j g h_j) \right|^n \quad (4)$$


A value of 0.83 is employed for  $C_{ij}$ , and  $n$  is set to 0.5 [17]. This means that the airflow from control volume  $i$  to control volume  $j$  is modelled as if the flow passes through a small opening with sharp edges (discharge coefficient = 0.64).

The global system of equation formed by mass balances, enthalpy balances, and state equations, is solved step-by-step and iteratively

1. air densities are calculated with the perfect gas law;
2. the pressure field is derived from the non-linear system of equations formed by the mass balance equations. For this, a step-relaxing method of the Newton–Raphson method is used [18,19];
3. the air temperature field is calculated by solving the linear system formed by the enthalpy balance equations.

## 2.2. Envelope model

The envelope model is based on the energy balance equation for each face of the envelope. Conductive and convective fluxes are given with unknown surface temperatures. Radiative longwave fluxes are given in scalar form using the surface temperature values computed at the previous iteration. Conductive heat fluxes are computed with response factors. This way, surface energy balances become linear equations with the unknown surface temperatures.

### 2.2.1. Sun patch model

AIRGLAZE computes the geometric shape of the sun patch. The first step in computation consists in projecting the obstructions on the exterior face of the building's envelope following solar beam direction. The shadowed part of the exterior face of the building's envelope may thus be determined. To track the sun patch inside the building, the sunny parts of glazed areas are projected on the interior walls following the direction of the solar beam. The sun patch is reconstituted by meshing the windows and projecting every centre of mesh on the interior walls following the solar beam direction. Each beam passing through a window mesh is assigned to the face of the interior wall containing the projected centre of the window mesh. The sun patch location and the values of shortwave radiation absorbed fluxes are computed at each time-step of the simulation.

### 2.2.2. Internal distribution of shortwave radiation

The computation of the internal distribution of the shortwave radiation used in AIRGLAZE takes the multiple

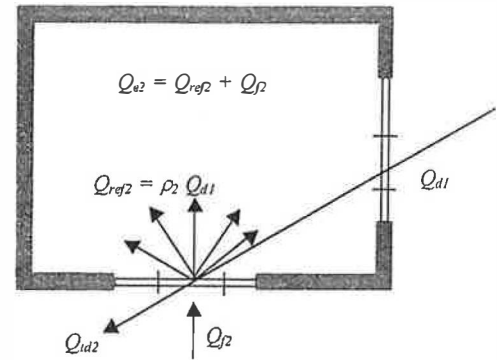


Fig. 3. Definitions of  $Q_e$ ,  $Q_{ref}$ ,  $Q_{id}$  and  $Q_f$  [3].

reflections, direct retransmission, reflection to the outside and transmission to other zones into account [3]. Assuming that the reflection is diffuse on the interior surfaces of the building, the computation of the internal repartition of shortwave radiation on the different interior surfaces is similar to the computation of the net longwave fluxes made with the radiosity method [20]. The unique difference when shortwave net fluxes are computed lies in the presence of some source or sink terms of diffuse radiation coming in through the glazed areas of the envelope ( $Q_f$  in Fig. 3). By analogy with the emittance defined as the LW source term emitted by a surface, the total SW source flux  $Q_{ek}$  (Eq. (5)) emitted by the interior face of surface  $k$  is used (Fig. 3).

$$Q_{ek} = Q_{fk} + Q_{refk} \quad (5)$$

$$Q_i = \sum_{k=1}^N (F_{ki} Q_{ek} + F_{ki} \rho_{SW,f,k} Q_k) \quad (6)$$

$N$  unknown net fluxes  $Q_i$  incident on surface  $i$  are obtained by solving a linear system made of the  $N$  balance Eq. (6) type equations.

At each time-step, this method needs to solve a linear system of  $N$  equations. However, note that the  $Q_{ek}$  only have to be computed at each time-step. The matrix of the linear system remains the same throughout the simulation; it is LU decomposed [19] at the beginning of the simulation only.

### 2.2.3. Internal distribution of longwave radiation

The Gebhart method [20] is used to compute net longwave radiation fluxes absorbed by the interior faces of the building envelope. The Gebhardt coefficient  $G_{ij}$  is defined as the ratio of the flux incident on surface  $j$  (directly or after multiple reflections) by the flux emitted by surface  $i$ .  $G_{ij}$  is linked to other coefficients  $G_{kj}$  by Eq. (7).

$$G_{ij} = F_{ij} + \sum_{k=1}^N F_{ik} \rho_{LW,k} G_{kj} \quad \forall (i, j) \in [1, N] \times [1, N] \quad (7)$$

$G_{ij}$  are computed by solving the linear system formed by  $N^2$  equations derived from Eq. (7). Net longwave fluxes absorbed by face  $i$  ( $\Phi_{LW,i}$ ) are obtained from  $G_{ij}$  coefficients

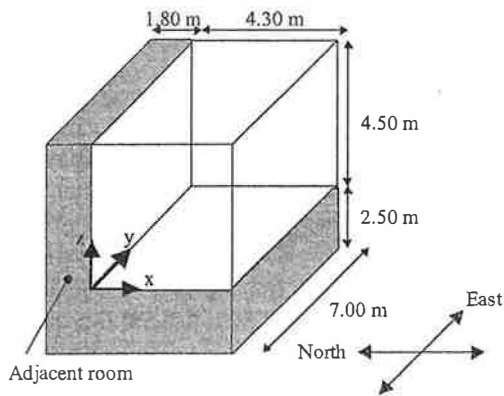


Fig. 4. Geometry of the experimental IEA Annex 26 atrium.

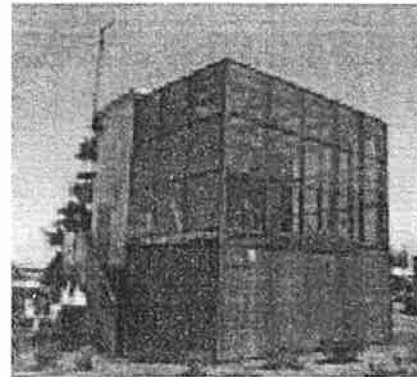


Fig. 6. The experimental atrium (Yokohama, Japan) used in IEA Annex 26.

and surface temperatures with Eq. (8):

$$\Phi_{LW,i} = \sigma_0 \left( \sum_{k=1}^N (\alpha_{LW,i} G_{ki} - \delta_{ik}) \epsilon_k A_k T_{wall,k}^4 \right) \quad (8)$$

The linear system of equations yielded by the Gebhardt method is larger than that of the radiosity method.  $N \times N$  linear equations (as opposed to  $N$ , for the radiosity method) have to be solved. However, the key advantage of the Gebhardt method is that the  $G_{ij}$  coefficients are independent of surface temperature. Therefore, they are calculated for one given geometry and one given set of wall reflectivities. Conversely, radiosities would have to be computed at each time-step by solving of a linear system of  $N$  equations. As a result, the Gebhardt method becomes of increasing interest as simulations are made over long periods of time.

### 3. Zonal simulation of IEA Annex 26 experimental building

An experimental atrium (see Fig. 6) was built in Yokohama, Japan, in the framework of IEA Annex 26 ‘Air Flow Patterns in Large Enclosures’ [15]. The main objective of this experimental program was to obtain boundary conditions and experimental data to test the capabilities of CFD

and macroscopic models to describe thermal and air velocity fields in atrium buildings. Fig. 4 presents the geometry of the atrium studied within this IEA Annex. Different ventilation and air cooling strategies were tested. Stratified conditions were very difficult to achieve during sunny periods, most of the ventilation scenarios leading to nearly fully-mixed conditions. However, the analyses reported herein are based on a ventilation strategy that yielded stratified conditions: the atrium was cooled and mechanically ventilated, supply and exhaust vents being located on the lower part of the north wall (see Fig. 5). Air and interior surface temperatures were measured at different locations in the room. They were made every 5 min and averaged over 1 h. The experimental data available from this study is not practical for performing simulations with a code like AIRGLAZE; external surface temperatures were not measured on all walls, and the floor had a hollow structure for which the calculation of the response factors is rather delicate. However, it is easy to extract boundary conditions to test a CFD or a zonal model.

#### 3.1. Numerical simulations with AIRGLAZE

We simulated this building with the zonal module of AIRGLAZE for 4 September 1994. This day was very sunny, and stable thermal stratification in the room was achieved. The simulation used a grid of 7  $x$ -direction cells,

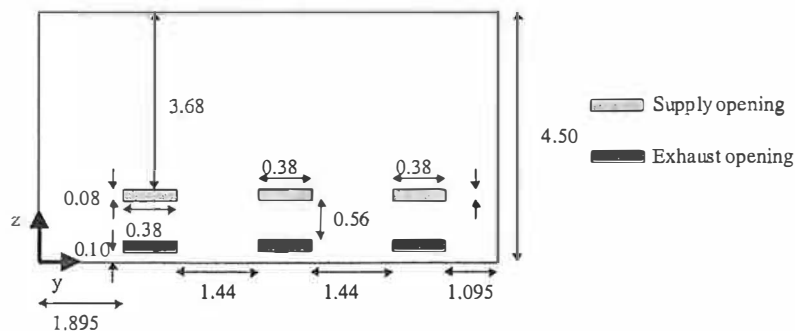


Fig. 5. Positions of air supply and exhaust openings in IEA Annex 26 atrium (m).

12  $y$ -direction cells, and 10  $z$ -direction cells. Inner surface temperatures, inlet air temperature and steel frame temperatures were used as boundary conditions. Hence, the envelope model, sun patch model, and the internal shortwave radiation model were not tested. Previous studies on this atrium [21] showed that heat gains due to atrium steel beam structural frame insolation must be taken into account in temperature and airflow simulations. In our simulations, these heat gains were distributed according to the beam positions in the room and their surface temperatures measured at three locations. Although the air velocity at the supply opening is  $1.4 \text{ m s}^{-1}$ , no particular jet model was used to describe the inlet zone. Air infiltration was neglected in the simulations. A constant convection heat transfer coefficient ( $3.0 \text{ W m}^{-2} \text{ K}^{-1}$ ) was first used to describe convection heat transfers between the interior air volume and the inner surfaces of the walls or the steel beams. We also used temperature-dependent heat transfer coefficients (cf. Section 3.4 and IEA Annex 26 [15]). It took about 12 h to simulate 24 h of real time using a time-step of an hour on a Pentium 450 MHz PC with 256 MB RAM.

Fig. 7 shows good agreement between the average of the 27 measured air temperatures and those of the calculated air temperatures in the 27 cells that include the sensor locations. The average discrepancy between zonal and experimental average temperatures is lower than  $0.5^\circ\text{C}$ . Fig. 8 provides a comparison of numerical and experimental air temperature at different heights at the centre of the room. Thermal stratification is quite significant; the measured temperature difference between 1.0 and 3.8 m at 11:00 h is  $8.8^\circ\text{C}$ ; numerically, the corresponding temperature difference

(between the cells whose centres are at 1.16 and 3.75 m) is  $7.6^\circ\text{C}$ .

The temperature at the lowest sensor location ( $z = 1.0 \text{ m}$ ) is overestimated by AIRGLAZE during the night (19:00–06:00 h) on average by  $1.4^\circ\text{C}$  (Fig. 8). This may be due to poor modelling of the cold jet entering the room. This has a greater effect during the night as the air motion inside the room is mostly driven by this jet during these periods. The analysis of the air velocity fields during the day showed that the air movements in the lower part of the atrium were increased when the atrium was exposed to solar radiation. This confirms that natural convection is enhanced during these periods.

Experimental and numerical results are generally in good agreement, except near the inlet at the lower part of the atrium. For the two upper sensors, the maximal and average temperature difference between experimental and numerical data is 0.9 and  $0.3^\circ\text{C}$  at 2.4 m, and 1.2 and  $0.4^\circ\text{C}$  at 3.8 m, respectively. Numerical results mostly lie within the error bars of the measurement data.

### 3.2. One-air-node approach comparison

In most thermal simulation tools, the interior air volume of a room is supposed to be fully-mixed and is represented by only one air temperature (homogeneous air temperature within the space). One-air-node temperature simulations are feasible with AIRGLAZE with minor modifications to the code. The zonal description of the interior air volume gives better results than the one-air-node temperature model for the upper part of the atrium. The difference between the two

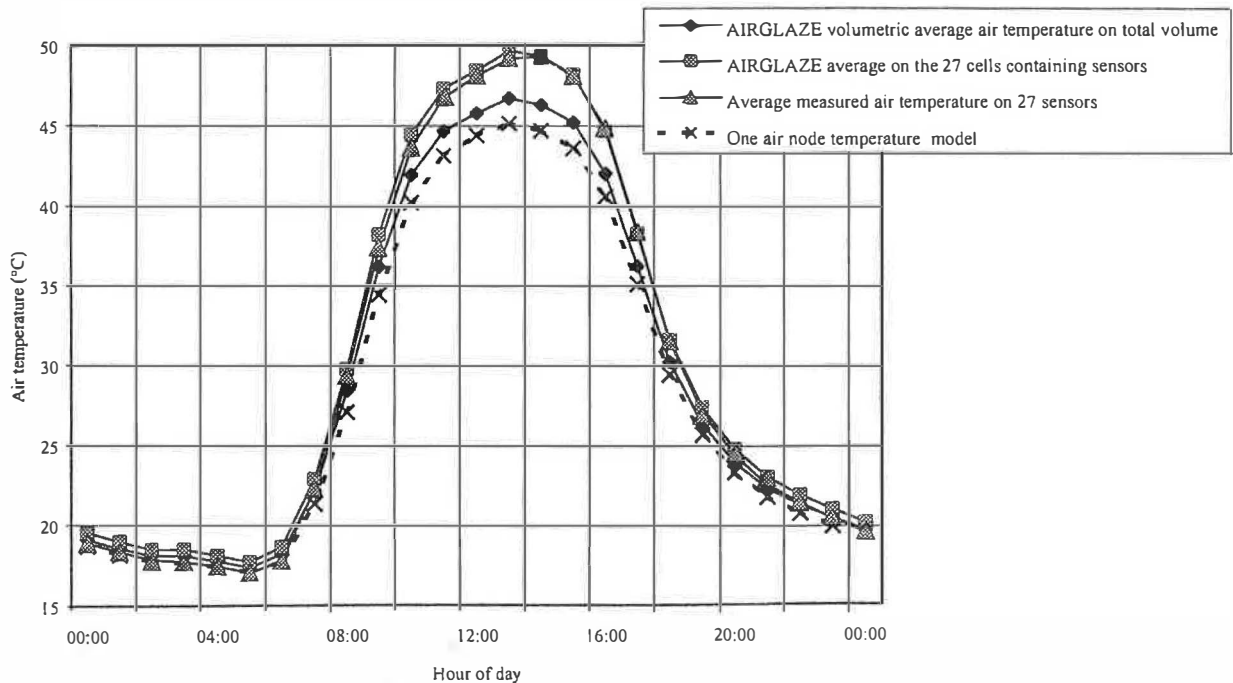


Fig. 7. Comparison between numerical and experimental averaged air temperature in IEA Annex 26 atrium. Simulation date: 4 September 1994.

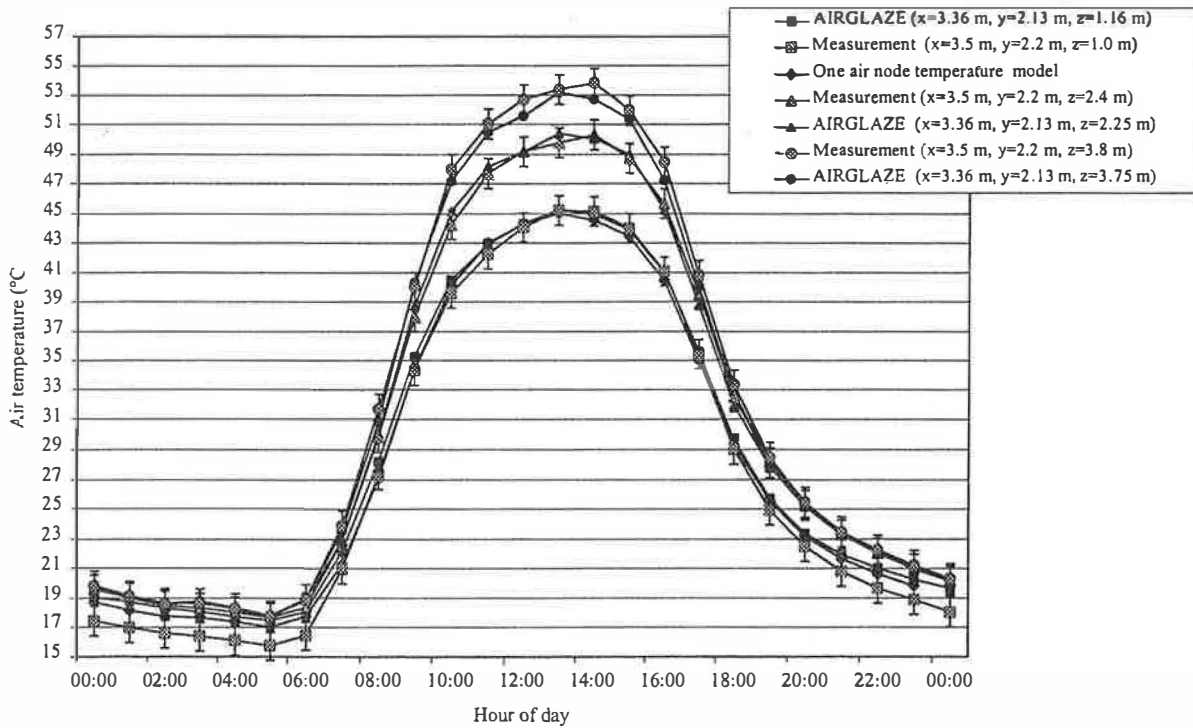


Fig. 8. Comparison between numerical and experimental air temperature at the centre of IEA Annex 26 atrium. Simulation date: 4 September 1994.

approaches at 13:00 h is greater than 4°C at 2.4 m, and 8°C at 3.8 m (Fig. 8). Besides, using a one-air-node approach yields an air temperature that is very significantly lower in the atrium (4.6°C at 14:00 h) than the average of the measured air temperatures at the 27 locations (Fig. 7).

### 3.3. Influence of spatial discretization

We refined the  $z$ -direction grid to test the influence of the vertical spatial discretization. Except for the cells corresponding to the supply and exhaust openings, the cell heights were divided by 2, yielding an average cell height of 0.25 m.

The impact of the grid refinement on the simulation results is relatively large for the lower sensor (1.1 and 2.3°C for mean and maximum discrepancies between both simulations). This is mostly due to local effects of the jet such as the predictably large temperature gradients near the supply zone. However, averages on several cells around the sensor location show much better agreement. The mean and maximum discrepancy between both simulations of the average air temperatures computed at the 27 sensor locations is of 0.4 and 0.9°C, respectively. For the two upper sensors located at the centre of the room, the mean and maximum discrepancy is lower than 0.1 and 0.7°C, respectively.

### 3.4. Influence of convective heat transfer coefficients

Convective heat transfer coefficients are difficult to estimate in real building enclosures. Correlations for natural convection heat transfer coefficients available in the litera-

ture usually rely on the temperature difference between the surface and the air [22]. For the vertical surfaces, the heat transfer coefficients were set to  $h_c = 1.5|T_{\text{wall}} - T_{\text{air}}|^{1/3}$  (instead of  $3.0 \text{ W m}^{-2} \text{ K}^{-1}$ ) as in Annex 26 [15]. This change had very little impact on our simulations results. The maximum and mean discrepancies at the sensor locations between both simulations were of 0.5 and 0.15°C, respectively.

## 4. ENTPE test cell simulation using AIRGLAZE

### 4.1. Experimental facility

Experiments were performed at the Laboratoire des Sciences de l'Habitat (Building Science Laboratory), at ENTPE, Vaulx-en-Velin, France. The experimental test cell (SUNCELL) is presented in Fig. 9. It consists of a real

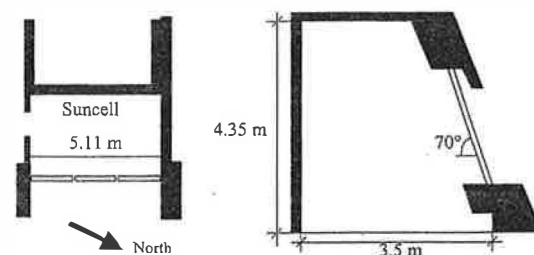


Fig. 9. Top view and side view of the ENTPE test cell (SUNCELL).

laboratory space of  $61 \text{ m}^3$  with an inclined facade; the cell is  $4.35 \text{ m}$  high, and has a large window of  $11 \text{ m}^2$  on its inclined facade. Due to the east–east–north orientation of the window, the SUNCELL receives direct solar radiation in the morning only. A  $35 \text{ mm}$  thick ‘raised-floor’ made of chip-board was installed on small wood beams laid on the original floor. The SUNCELL is mechanically ventilated at  $6 \text{ ACH}$  by extraction in the upper part of the room. The exterior air is sucked into the room through a rectangular opening in the lower part of the window. Some work was performed to improve the airtightness of the envelope. Subsequent pressurization tests showed that the resulting airtightness was of about  $8.5 \text{ l s}^{-1}$  at  $4 \text{ Pa}$ .

Sixteen surface and seven air temperature sensors (PT 100 sensors) were installed in the SUNCELL (Fig. 10). Each air temperature sensor was shielded with two co-axial chrome cylinders. Eight surface temperature sensors were located on the lower side of the ‘raised-floor’. The exterior air temperature and the exterior surface temperature of the window were also measured. Air temperature sensors were placed on two manually movable masts. The accuracy of the temperature measurements was estimated to be  $\pm 0.3^\circ\text{C}$ . Horizontal global and diffuse irradiances were measured by the ENTPE meteorological station located on the roof of the building. Measurements were made every minute and averaged over  $5 \text{ min}$ .

Fig. 11 presents the evolution with time of measured air temperatures during a period where the SUNCELL was not

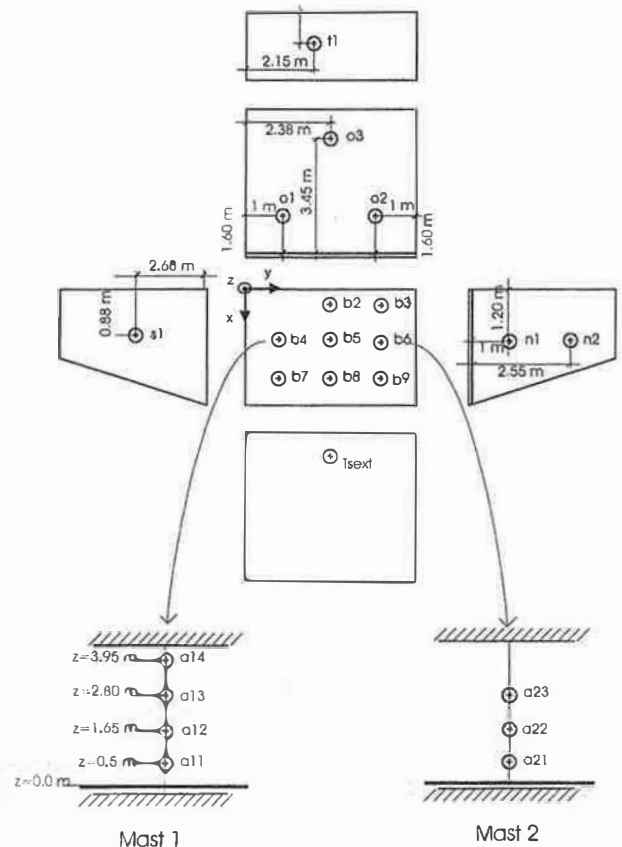


Fig. 10. Locations of temperature sensors in the SUNCELL.

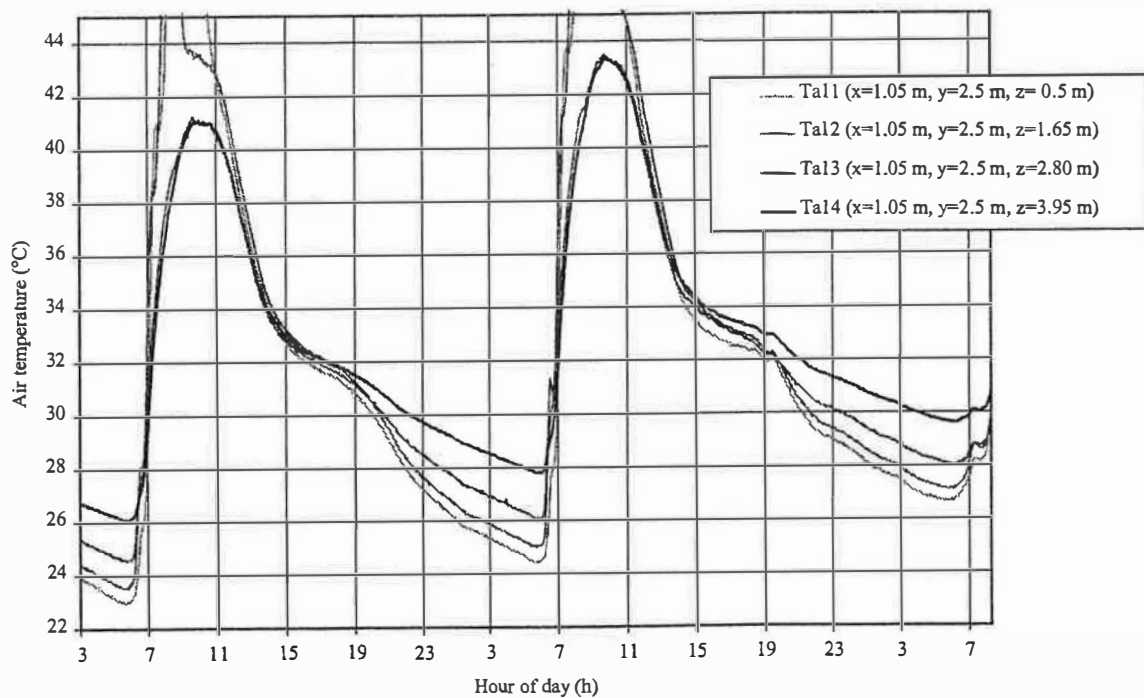


Fig. 11. Measured air temperatures on mast 1 ( $x = 1.05 \text{ m}$  and  $y = 2.5 \text{ m}$ ). Sunny days. Simulation date: 20 and 21 June 1998. Mechanical ventilation OFF.



mechanically ventilated. (Note that, despite the chrome cylinders, we observed the overheating of air temperature sensors Ta11 and Ta12 in sunny conditions. The corresponding measurement data is not used in this paper). It appears that thermal stratification occurs during the night, and is not affected by mechanical ventilation. Thermal stratification during the night is low: the maximum temperature difference ( $2.7^{\circ}\text{C}$ ) between top and lower part of the cell (Ta14 and Ta11) is reached at 05:40 h.

#### 4.2. Overview of simulations of SUNCELL

The grid used to simulate the SUNCELL is included in a parallelepiped that has 12  $x$ -direction cells, 10  $y$ -direction cells and 8  $z$ -direction cells. This results in a computational domain that has 816 cells. (Note that some cells of the parallelepiped are excluded from the computational domain because the front-window is inclined.) In the airflow model, a fixed pressure boundary condition is used for the opening in the window. The supply air temperature is set to the exterior air temperature, and a volumetric airflow rate is set at the air outlet. Surface temperatures measured in the room were used as boundary conditions for the envelope model, except for the floor where surface temperatures measured on the external side were used, and for the window for which the outside air temperature was used. The time-step was set to 5 min for the simulations. Two periods where the SUNCELL was highly insulated were tested. In the first one, the SUNCELL was mechanically ventilated whereas, during the second period, the SUNCELL was not ventilated. Simula-

tions were run on a Pentium II 333 MHz PC with 128 MB RAM. About 1 h of computation time was needed to simulate 1 h of real time with a time-step of 5 min.

We compared the evolution in time of the measured and calculated air temperatures at  $x = 1.05$  m and  $y = 2.5$  m in the coordinates system of Fig. 10, at different heights in the room.

#### 4.3. Case 1: SUNCELL not ventilated

In this case, the supply and exhaust openings were sealed. Fig. 12 shows that the AIRGLAZE model can predict the time periods of stratified air temperature fields. Agreement between numerical and experimental data is good during stratified periods (20:00–06:00 h). The average discrepancy between (a) the zonal and experimental results, and (b) the one-air-node and experimental results is of  $0.4$  and  $1.0^{\circ}\text{C}$ , respectively. This suggests that the zonal approach improves the prediction of the thermal behaviour of this space. Note also that the thermal gradient between the lower and upper parts of the cell is not very significant (the maximum temperature difference between sensor Ta1 and Ta4 is  $3.4^{\circ}\text{C}$  at 05:50 h). The improvements due to the zonal model are expected to be even more significant with greater thermal stratification.

The airflow obtained at different time-steps (Fig. 13) shows that the sun patch in the SUNCELL puts the air in motion and yields fully-mixed conditions. This is consistent with the findings reported in IEA Annex 26 [15] as stratified conditions were very difficult to obtain during sunny periods in the experimental atrium in Yokohama.

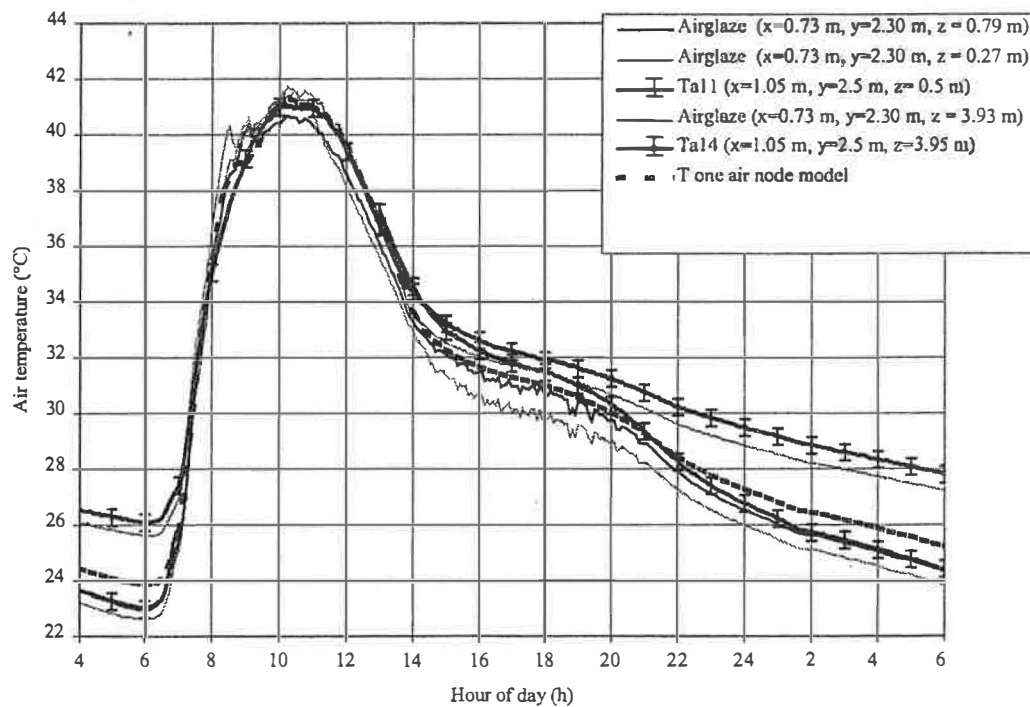


Fig. 12. Measured and simulated air temperatures. Sunny day. Simulation date: 20 June 1998. Mechanical ventilation OFF. For clarity, error bars are represented every 60 min.

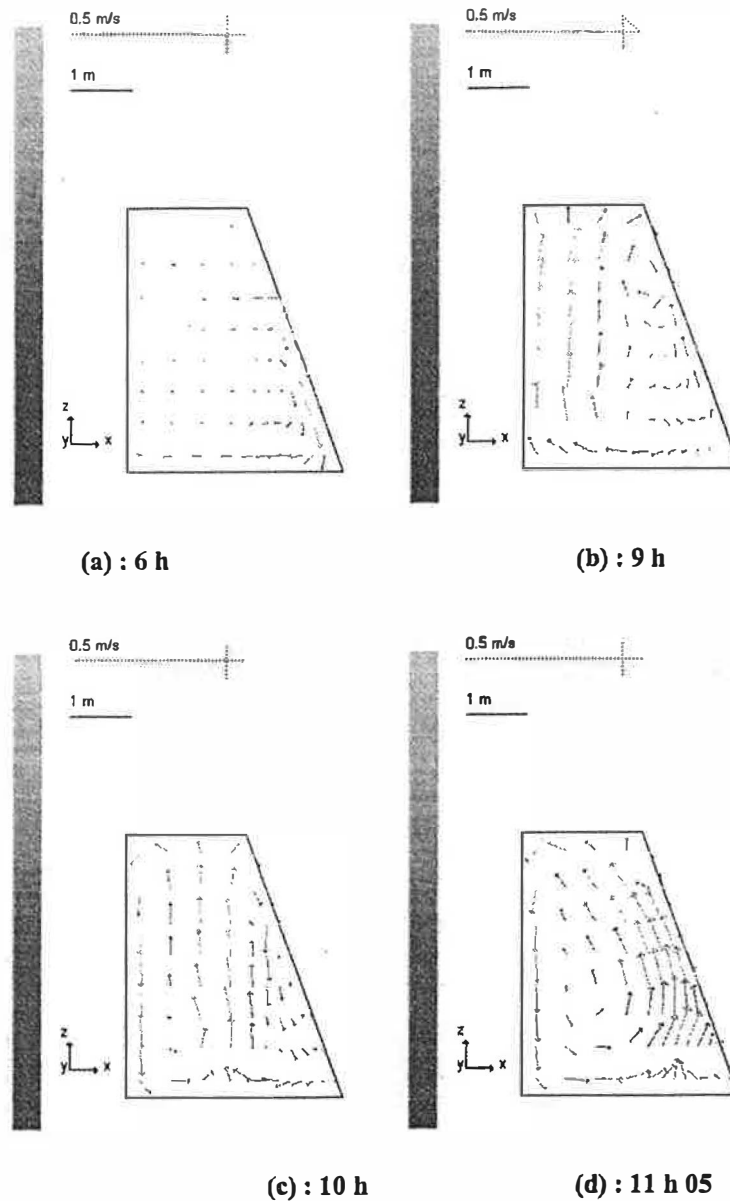


Fig. 13. Evolution with time of the velocity fields in plan ( $y = 2.30$  m) obtained by AIRGLAZE at different time-steps when the SUNCELL is highly sunny and not ventilated. Day simulation: 20 June 1998.

#### 4.4. Case 2: mechanically ventilated SUNCELL

The comparison of numerical with experimental results for the case where the SUNCELL is mechanically ventilated confirms the analyses made for Case 1. Again, the model accurately finds the stratified periods. However, the agreement between numerical and experimental results is not as good as in Case 1 in the lower part of the cell (Fig. 14). As for the IEA Annex 26 atrium, this could be explained by the poor representation of the jet zone in the zonal airflow model.

For the upper part of the SUNCELL ( $z > 1.8$  m), when the temperature field is stratified (Fig. 14), the zonal model is clearly beneficial compared to the one-air-node for predicting the thermal behaviour of the test cell.

#### 5. Conclusion

The governing heat transfer phenomena encountered in large highly-glazed spaces are significantly different than those encountered in conventional buildings. However, because existing building thermal simulation codes were originally developed for conventional buildings, they seem inappropriate to predict the thermal and airflow behaviour of large highly-glazed spaces. We have developed a new model (AIRGLAZE) capable of representing the transient air temperature and airflow fields in large highly-glazed spaces. The model is based on the coupling of a zonal airflow module with an envelope module that accurately models the sun patch and the internal distribution of shortwave and longwave radiation in the building.

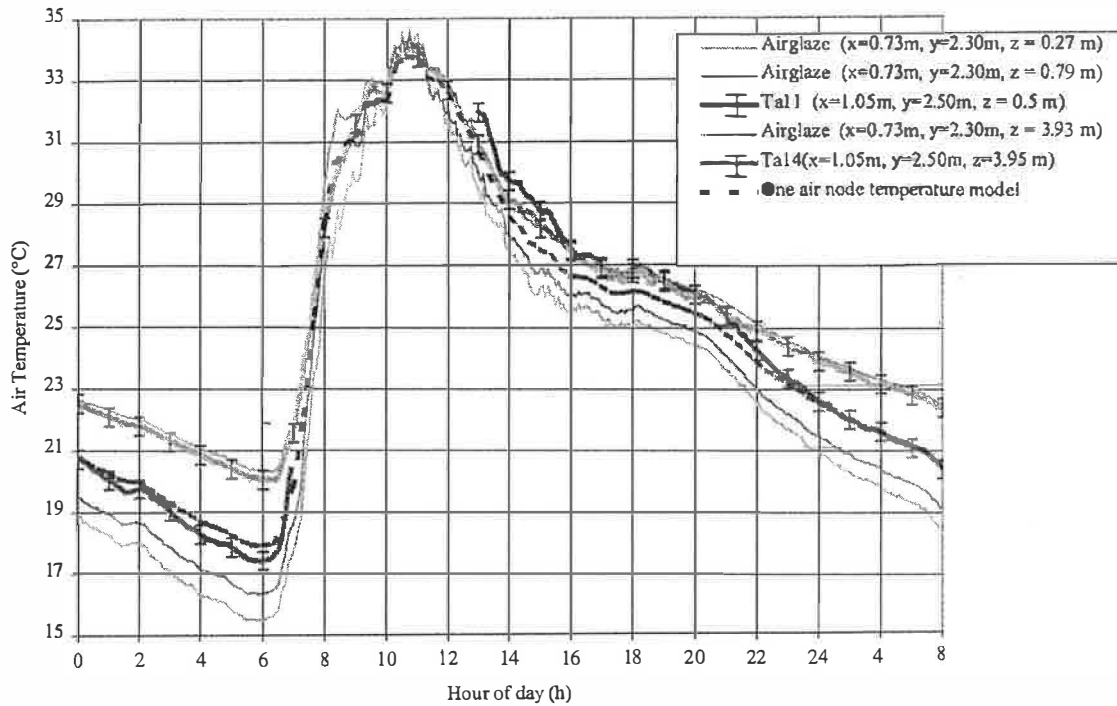


Fig. 14. Measured and simulated air temperatures. Sunny day. Simulation date: 18 June 1998. Mechanical ventilation ON. For clarity, error bars are represented every 60 min.

Measurement data from two experimental test cells were used to evaluate the accuracy of AIRGLAZE for predicting the air temperature fields. Both comparisons show good agreement between experimental and numerical results. However, one should keep in mind that the use of surface temperatures for some of the boundary conditions simplifies considerably the simulations, especially in the case of the Yokohama atrium. The time periods corresponding to stratified and fully-mixed conditions are accurately found by the model. Besides, air temperature simulation data agrees well with measurement results. In both cases, the zonal approach clearly improves the air temperature prediction during stratified periods. However, in both cases, the greatest discrepancies in the results are found near the inlet zone. This could be improved with a better modelling of the momentum-driven zones (e.g. jet zones) [23–25].

In the IEA Annex 26 experimental atrium, the number of cells in the vertical direction was increased to see the potential impact of a different grid on the simulation results. This change did not have a major effect on the average temperature in the room. Although these results look promising, additional work is needed in this area to derive rules-of-thumb with respect to spatial discretization.

The simulation results on the IEA atrium are not very sensitive to the convective heat transfer coefficients. In a way, this is reassuring as large uncertainties are usually associated with this input data (e.g. because they are derived for geometries that differ significantly from those of interest).

The simulations on the SUNCELL were run without tuning the input parameters (e.g. the heat exchange coefficients). Additional work is underway to perform sensitivity analyses on the input parameters to derive confidence intervals for simulation output data. Further work is also needed to evaluate the AIRGLAZE model on larger spaces; however, collecting good thermal and airflow measurement data on large highly-glazed buildings over significant periods of time remains a challenge.

#### Acknowledgements

The authors would like to thank Véronique Richalet for her valuable advice on existing thermal simulation tools; Olivier Dazel for his contribution in the implementation of the model; and Dr. Kato (University of Tokyo) for the experimental data on the IEA Annex 26 experimental atrium in Japan.

#### References

- [1] Y. Bryn, Atrium buildings from the perspective of function indoor air quality, and energy use, *ASHRAE Trans.* 101 (2) (1995) 829–840.
- [2] K.J. Lomas, H. Eppel, Atrium studies technical review, Final report: Environmental Computer Aided Design and Performance (ECADAP) Group School of the Built Environment, 1994, ETSU S/N6/00209/REP.

- [3] H. Pfrommer, Thermal Modelling of Highly Glazed Spaces, De Montfort University, Leicester, 1995. 229 p.
- [4] J.A. Clarke, J. Hand, P. Strachan, J.L.M. Hensen, Esp-r, a building and plant energy simulation research environment, Energy Simulation Research Unit, University of Strathclyde, Glasgow, 1991, 186 p. Manual U91/2.
- [5] P.T. Lewis, D.K. Alexander, HTB2 — A Model for the Thermal Environment of Buildings in Operation, Users Manual Release 1 Rev.0, Welsh School of Architecture, Cardiff, UK, 1985, 154 p.
- [6] M. Wall, A design tool for glazed spaces, Part I. Description, ASHRAE Trans. 101 (2) (1995) 1261–1271.
- [7] L. Serres, Etude de l'impact d'une perturbation thermique locale de type tache solaire. Influence sur le confort thermique, Doctorat: Génie Civil, Institut National des Sciences Appliquées de Toulouse, 1997, 148 p.
- [8] A. Trombe, L. Serres, M. Begues, Enclosure Internal Solar Radiation Distribution, in: ISES 1997 Solar World Congress, 1997.
- [9] A. Laouadi, M. Atif, Comparison between computed and field measured thermal parameters in an atrium building, Building & Environ. 34 (2) (1999) 129–138.
- [10] Solar Energy Laboratory, TRNSYS. A Transient Simulation Program. User Manual, Madison, USA, University of Wisconsin, MD, 1995.
- [11] A. Voeltzel, Modélisation du comportement thermo aéraulique des grands volumes vitrés en régime dynamique, Doctorat: Conception en Bâtiment et Techniques Urbaines, Institut National des Sciences Appliquées de Lyon, 1999, 234 p.
- [12] P.G. Schild, P.O. Tjelflaat, D. Aiulfi, Guidelines for CFD modeling of atria, ASHRAE Trans. 101 (2) (1995) 1311–1332.
- [13] D. Groleau, C. Marenne, M. Lefeuve, Simulation des écoulements d'air dans les espaces vitrés ensoleillés: le cas d'une rue couverte, in: European Conference on Energy Performance and Indoor Climate in Buildings, Lyon, Vol 1, 1994, pp. 161–166.
- [14] S. Kato, S. Murakami, S. Shoya, F. Hanyu, J. Zeng, CFD analysis of flow and temperature fields in atrium with ceiling height of 130 m, ASHRAE Trans. 101 (2) (1995) 1144–1160.
- [15] IEA. Annex 26: Ventilation of large spaces in buildings. Part 3. Analysis and Prediction Techniques. (Draft), Paris: IEA. Energy Conservation in Buildings and Community Systems, 1996, 256 p.
- [16] M. Sherman, A Power-law formulation of laminar flow in short pipes, J. Fluids Eng. 114 (1992) 601–605.
- [17] E. Wurtz, Modélisation tridimensionnelle des transferts thermiques et aérauliques dans le bâtiment en environnement orienté objet, Doctorat: Sciences et Techniques du Bâtiment, Ecole Nationale des Ponts et Chaussées, 1995, 206 p.
- [18] M.K. Herrlin, F. Allard, Solution methods for the air balance in multizone buildings, Energy and Buildings 18 (2) (1992) 159–170.
- [19] W.H. Press, S.A. Teukolsky, W.T. Vetterling, B.P. Flannery, Numerical Recipes in Fortran. The Art of Scientific Computing, 2nd Edition, Cambridge University Press, Cambridge, 1992, 963 p.
- [20] Y. Jaluria, K.E. Torrance, Computational Heat Transfer, Hemisphere, New York, 1986. 366 p.
- [21] T. Hiramatsu, T. Harada, S. Kato, S. Murakami, H. Yoshino, Study of Thermal Environment in Experimental Real-scale Atrium, in: ROOM VENT'96, Yokohama, Japan, 1996.
- [22] E. Dascalaki, M. Santamouris, C.A. Balaras, D.N. Asimakopoulos, Natural convection heat transfer coefficients from vertical and horizontal surfaces for building applications, Energy and Buildings 20 (3) (1994) 243–249.
- [23] H. Bouia, Modélisation simplifiée d'écoulements de convection mixte interne: Application aux échanges thermo-aérauliques dans les locaux, Doctorat: Mécanique des Fluides, Faculté des Sciences Fondamentales et Appliquées, Poitiers, France, 1993, 110 p.
- [24] C. Inard, H. Bouia, P. Dalicieux, Prediction of air temperature distribution in buildings with a zonal model, Energy and Buildings 24 (2) (1996) 125–132.
- [25] E. Wurtz, J.M. Nataf, F. Winkelmann, Two-and three-dimensional natural and mixed convection simulation using modular zonal models in buildings, Int. J. Heat Mass Transfer 42 (5) (1999) 923–940.